




OPEN ACCESS

Technical note on the exploration of COVID-19 in autopsy material

Matthew Phillip Humphries ^{1,2}, Victoria Bingham,¹ Fatima Abdullah Sidi,¹ Stephanie Craig,¹ Beatriz Lara,³ Hesham El-daly,³ Nicole O'Doherty,⁴ Perry Maxwell,⁵ Claire Lewis,⁶ Stephen McQuaid,⁶ James Lyness,⁴ Jacqueline James,⁶ David R J Snead,⁷ Manuel Salto-Tellez^{1,8}

► Additional supplemental material is published online only. To view, please visit the journal online (<http://dx.doi.org/10.1136/jcp-2022-208525>).

¹Precision Medicine Center of Excellence, Queen's University Belfast, Belfast, UK

²National Pathology Imaging Cooperative, Leeds Teaching Hospitals NHS Trust, Leeds, UK

³University Hospitals Coventry and Warwickshire NHS Trust, Coventry, UK

⁴Northern Ireland State Pathologist's Department, Belfast, UK

⁵Northern Ireland Molecular Pathology Laboratory, Queen's University Belfast, Belfast, UK

⁶The Patrick G Johnston Centre for Cancer Research, Queen's University, Northern Ireland Biobank, Belfast, UK

⁷Pathology, University Hospitals Coventry and Warwickshire NHS Trust, Coventry, UK

⁸Division of Molecular Pathology, The Institute of Cancer Research, London, UK

Correspondence to

Professor Manuel Salto-Tellez, Precision Medicine Centre of Excellence, Queen's University Belfast, Belfast, UK; m.salto-tellez@qub.ac.uk

Received 15 August 2022

Accepted 17 October 2022



© Author(s) (or their employer(s)) 2023. Re-use permitted under CC BY. Published by BMJ.

To cite: Humphries MP, Bingham V, Abdullah Sidi F, et al. *J Clin Pathol* Epub ahead of print: [please include Day Month Year]. doi:10.1136/jcp-2022-208525

ABSTRACT

Interrogation of immune response in autopsy material from patients with SARS-CoV-2 is potentially significant. We aim to describe a validated protocol for the exploration of the molecular physiopathology of SARS-CoV-2 pulmonary disease using multiplex immunofluorescence (mIF).

The application of validated assays for the detection of SARS-CoV-2 in tissues, originally developed in our laboratory in the context of oncology, was used to map the topography and complexity of the adaptive immune response at protein and mRNA levels.

SARS-CoV-2 is detectable *in situ* by protein or mRNA, with a sensitivity that could be in part related to disease stage. In formalin-fixed, paraffin-embedded pneumonia material, multiplex immunofluorescent panels are robust, reliable and quantifiable and can detect topographic variations in inflammation related to pathological processes.

Clinical autopsies have relevance in understanding diseases of unknown/complex pathophysiology. In particular, autopsy materials are suitable for the detection of SARS-CoV-2 and for the topographic description of the complex tissue-based immune response using mIF.

INTRODUCTION

SARS-CoV-2, first reported in Wuhan (China) in December 2019, was declared a global pandemic by the WHO in March 2020.¹

Following authoritative calls defending the potential key role of autopsy-based analyses in COVID-19,² we present herein a model for a molecular physiopathological analysis of COVID-19 autopsy samples. We include validations of the following approaches in challenging formalin-fixed, paraffin-embedded (FFPE) autopsy materials: immunohistochemistry (IHC) and RNA *in situ* hybridisation detection of SARS-CoV-2 and multiplex analysis of the immune response in the COVID-19 pneumonic process, with digital pathology quantitation.

METHODS

Materials

To validate COVID-19 detection, we used COVID-19-positive control FFPE macaque tissue from collaborators at Erasmus University in Rotterdam.³ To confirm the specificity of our tests, we analysed

64 lung biopsy and respiratory tract cytology samples, excluding COVID-19 pneumonia.⁴

In addition, we tested FFPE lung tissue taken at autopsy from two patients dying from pneumonia with positive COVID-19 PCR tests and from two patients who died of non-COVID-19-related pneumonia, with a time of disease development and autopsy performance well before December 2019. We refer to cases 1 and 2 as the two COVID-19 proven autopsy cases, while cases 3 and 4 represent patients who died with pneumonia (more than 6 months before the outbreak). The aetiology and lung pathology of each case is described in online supplemental data 1. A COVID-19-positive H&E is shown in [figure 1](#), where the physiopathology of several areas are illustrated: overview ([figure 1A](#)), a viral syncytial formation ([figure 1B](#)), DAD with re-epithelisation ([figure 1C](#)), vascular inflammatory changes ([figure 1D](#)) and minimal chronic interstitial inflammation ([figure 1E](#)).

In situ detection of SARS-CoV-2

Detection was conducted in the macaque animal model, the retrospective clinical samples pre-COVID-19 and in the four autopsy samples described. Three-micrometre-thick sequential sections were obtained from all blocks and stained for SARS-CoV-2 nucleoprotein IHC or V-nCoV2019-S RNAScope. Automated IHC was performed using a Leica BOND RX with a rabbit monoclonal antibody against SARS-CoV-2 nucleoprotein (40143-T62; Sino Biologicals, Pennsylvania, USA). IHC was optimised on known COVID-19-positive tissue.³ IHC required pretreatment with epitope retrieval solution 1 for 10 min at 100°C and a 1:2000 antibody dilution. Detection chemistry employed was BOND Polymer Refine Detection Kit (DS9800; Leica Biosystems, USA) or BOND Polymer Refine Red Detection Kit (DS9390, Leica Biosystems). RNAScope to detect viral mRNA was performed using a Leica Bond RX system using RNAScope 2.5 LS Probe to V-nCoV2019-S, nt: 21 631–23 303 (848568; Advanced Cell Diagnostics, USA). For assessment of RNA integrity, we used RNAScope 2.5 LS Positive Control Probe-Hs-UBC (312028, Advanced Cell Diagnostics). Detection chemistry employed was RNAScope 2.5 LSx Reagent Kit-BROWN (322100, Advanced Cell Diagnostics) or RNAScope 2.5 LS Reagent Kit-RED (322150, Advanced Cell Diagnostics). All sections

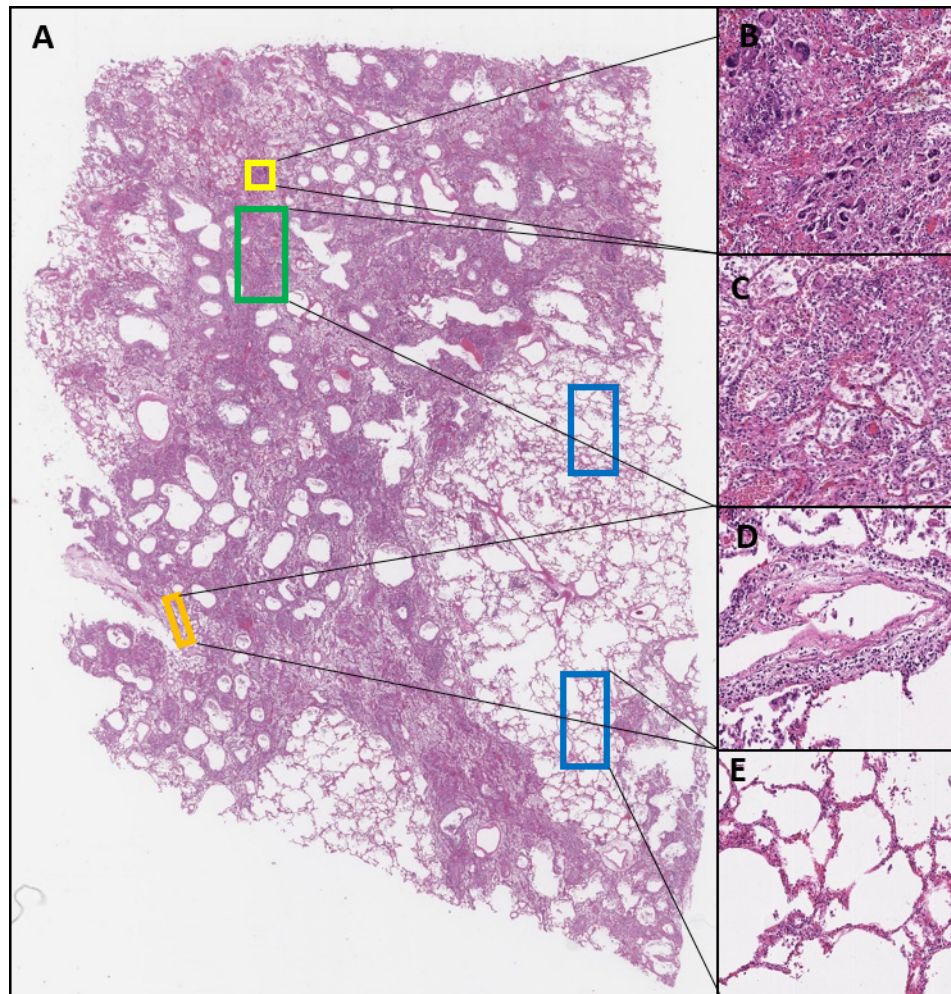


Figure 1 (A) Whole face H&E from COVID-19-positive autopsy case 2. (B) Illustration of an area of viral syncytial formation (yellow annotation), $\times 20$; (C) long-standing diffuse alveolar damage with re-epithelisation (green annotation), $\times 20$; (D) vascular inflammatory changes (orange annotation), $\times 20$; and (E) minimal chronic interstitial inflammation (blue annotations), $\times 20$.

were digitised using a Leica Aperio AT2 Scanner at $\times 40$ and analysed qualitatively and quantitatively *in silico* via Xplore (Philips) or the open source digital image analysis software programme QuPath V.0.2.0.⁵

Multiplex IHC fluorescence

Three-micrometer-thick sections were obtained from autopsy blocks and stained using two previously validated multiplex panels.^{6,7} Panel 1 assessed CD3 (T cells), CD4 (T-helper cells), CD20 (B cells) and CK (epithelial cells); panel 2 assessed PD-L1 (immune checkpoint marker), CD8 (cytotoxic T cells), CD68 (macrophages) and CK. Staining detection was performed using an Opal 7-Colour Automation IHC Kit (Akoya Biosciences, Marlborough, Massachusetts, USA). Antibody specifics and optimised retrieval methods for multiplex panels are detailed in online supplemental table S1. Opal fluorophores were used according to the manufacturer's instructions. All multiplex slides were digitised using a Vectra Polaris scanner (Akoya Biosciences) at $\times 20$.

Digital image analysis

3,3'-Diaminobenzidine (DAB) scan files captured on a Leica Aperio AT2 (.svs) or whole-slide Opal MOTiF fluorescence images captured on a Akoya Vectra Polaris (.qptiff) were

imported in to QuPath. Following precise annotation transfer from H&Es to the DAB and multiplex immunofluorescent images, a rigorous quality control process was undertaken by an experienced image analyst and histopathologist to ensure no spurious factors impacted extracted data, confirmed by a second reviewer, as previously reported.⁶⁻⁸

For multiplex immunofluorescence (mIF), cell detection was conducted using DAPI within annotated regions of interest (ROIs). Single-channel biomarker detection was carried out using positive cell detection features based on consensus thresholds across each panel using nuclear/cell Opal mean. Density per square millimetre data and overall positive cell count, expressed as a percentage, was extracted into Microsoft Excel.

RESULTS

In situ detection of SARS-CoV-2

Initially, we optimised COVID-19 IHC and RNAscope tests in positive control FFPE macaque tissue.³ Both tests were highly sensitive and specific in detecting SARS-CoV-2. SARS-CoV-2 was detected as expected by IHC and RNA-ISH in positive macaque control material (figure 2A,B). No evidence of SARS-CoV-2 by either IHC or RNA-ISH was seen in retrospective lung biopsy and lung cytology FFPE material (figure 2C,D,F,G).

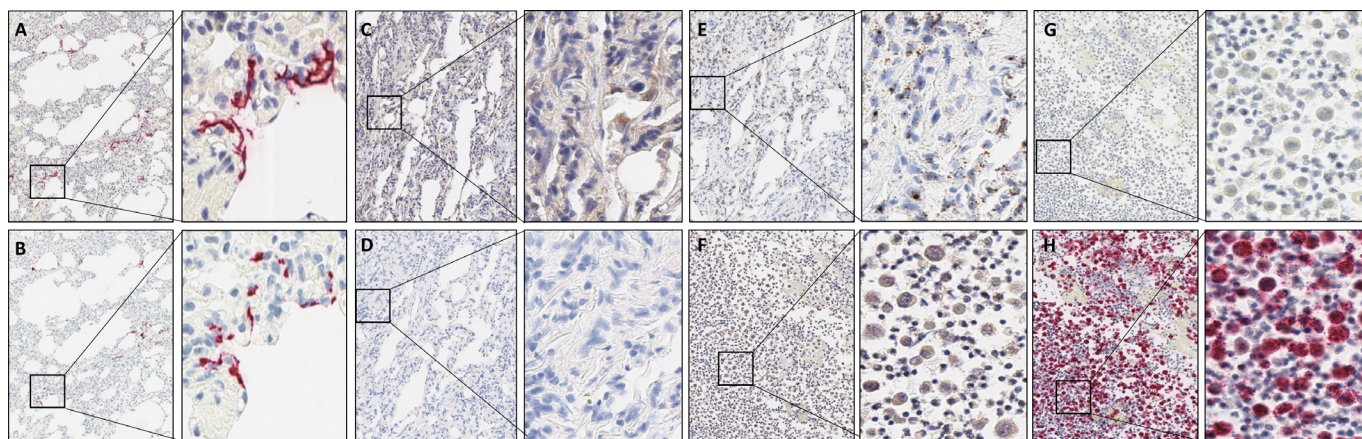


Figure 2 (A) Representative images showing SARS-CoV-2 nucleoprotein expression and (B) V-nCoV2019-S mRNA in FFPE macaque tissue. (C) Absence of SARS-CoV-2 nucleoprotein expression is depicted in lung biopsy FFPE and (F) lung cytology FFPE. (D) Absence of V-nCoV2019-S mRNA expression is depicted in lung biopsy FFPE and (G) lung cytology FFPE. (E) Positive control probe UBC mRNA expression is depicted in lung biopsy FFPE (reagent kit-BROWN) and (H) lung cytology FFPE (reagent kit-RED). All images are $\times 10$ magnification, with exploded views at $\times 40$. FFPE, formalin-fixed, paraffin-embedded.

RNA integrity was confirmed with positive control probe UBC (figure 2E,H).

All 64 clinically non-COVID-19 lung biopsy or cytology samples were negative for SARS-CoV-2 by IHC or RNAScope. In 7/50 cytology cell blocks, there was no expression of the RNAScope positive control probe UBC.

COVID-19 RNA and protein signals were not present in non-COVID-19 autopsy cases (cases 3 and 4). As depicted in figure 3, in autopsy case 1, numerous, scattered viral signals were identified by both IHC and RNAScope probe. Autopsy case 2 showed no positive IHC or RNA-ISH signals.

To test our protocol for future analysis of inflammation associated with specific detectable portions of viral RNA or protein,

we validated IHC and RNA-ISH detection in the context of DAB dual-plex and mIF, which was able to robustly detect SARS-CoV-2 in the macaque model and clinical autopsy 1 (online supplemental figure S1).

Capturing the immune microenvironment with multiplex IHC fluorescence

Application of multiplex immunofluorescent panels in autopsy material, previously optimised for our immune oncology studies,^{6,7} enabled us to delineate a range of immune cell phenotypes within COVID-19-positive material. To depict this visually, we chose two ends of the spectrum, namely, (1) an area

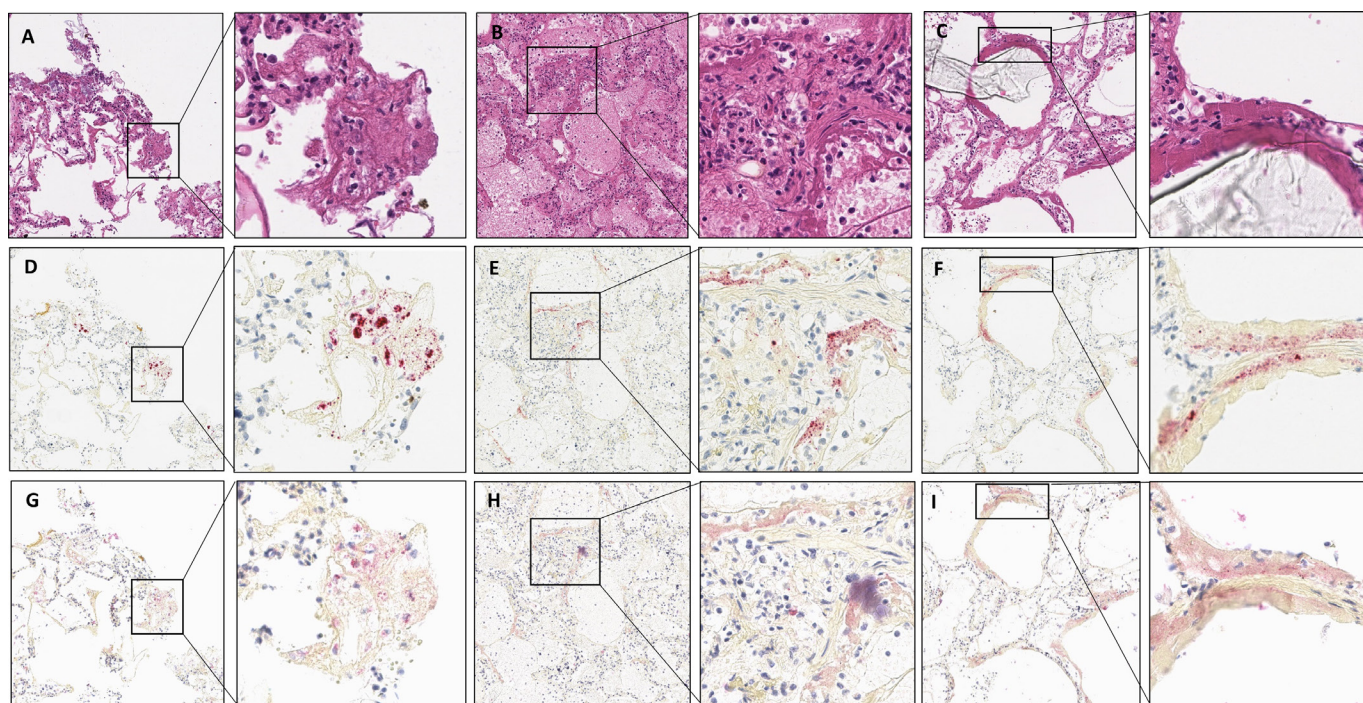


Figure 3 (A–C) Representative images showing H&E staining from COVID-19 autopsy case 1, (D–F) V-nCoV2019-S RNAScope and (G–I) SARS-CoV-2 nucleoprotein expression in three regions of FFPE autopsy tissue. All images are $\times 10$ magnification, with exploded views at $\times 20$. FFPE, formalin-fixed, paraffin-embedded.

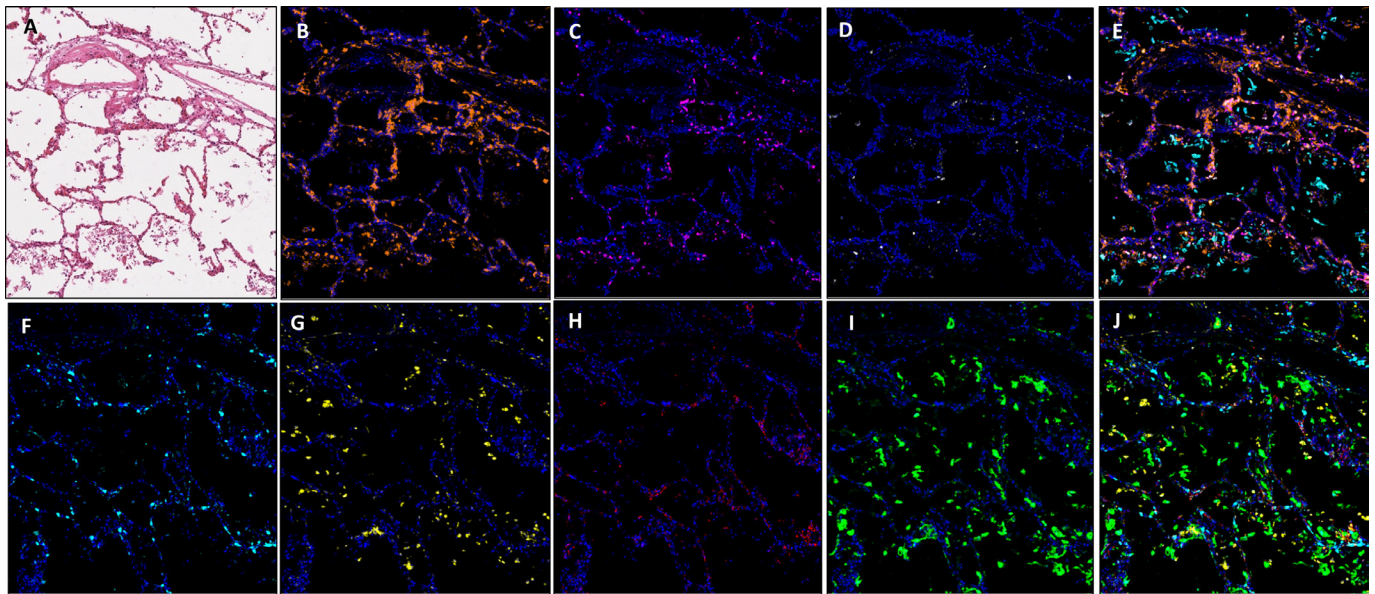


Figure 4 Images showing an area of minimal chronic interstitial inflammation in COVID-19 lung FFPE autopsy tissue case 1. (A) H&E; (B) CD3 (2GV6, orange); (C) CD4 (SP35, purple); (D) CD20 (L26, white); (E) composite CD3/CD4/CD20/CK and DAPI; (F). CD8 (C8/144B, aqua); (G). CD68 (514H12, yellow); (H) PD-L1 (SP263, red); (I) CK (AE1/AE3, green); and (J) composite CD8/CD68/PD-L1/CK and DAPI. All images are $\times 20$ magnification. FFPE, formalin-fixed, paraffin-embedded.

of minimal chronic interstitial inflammation (figure 4) and (2) a heavily inflamed area (figure 5). Here we specifically quantified total cell number and density per square millimetre for each biomarker and were able to analyse comparative expression of cell types using our robust digital pathology workflow.

In comparison to normal/near normal areas within COVID-19-positive case 2, ROIs representing diffuse damage contained a markedly increased expression of CD3, CD4 and CD68, in terms of density per square millimetre (online supplemental file 1). It was observed that while there was an increase in overall cell density in the ROI representing diffuse damage, the percentage distribution between ROIs was similar (figure 6). The exception

to this observation was a marked reduction in overall percentage of CD8-positive cells, which fell from 17.8% in the minimal chronic interstitial inflammation ROI to 5.7% in the areas with diffuse inflammatory damage (figure 6B).

As expected, areas of extensive pneumonia and oedema have a high density of CD68 expressing macrophages. In areas displaying vascular changes in all samples, the highest expressed markers in our panel were CD3 and CD4. In all ROIs, density of CD8-positive cells was higher in areas of normal/near normal when compared with areas of substantial change, that is, viral syncytium, extensive inflammation/pneumonia, vascular changes and established hyaline diffuse damage membrane formation

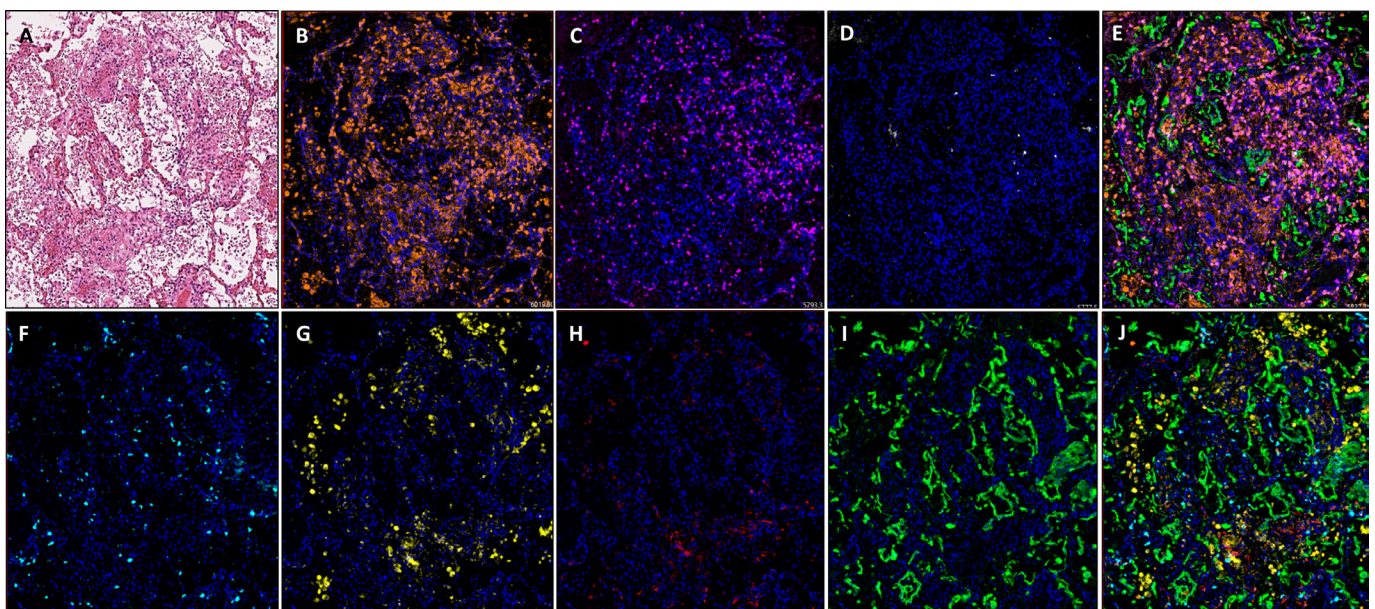


Figure 5 Images showing diffuse damage in COVID-19 lung FFPE autopsy tissue. (A) H&E, (B). CD3 (2GV6, orange); (C) CD4 (SP35, purple); (D) CD20 (L26, white); (E) composite CD3/CD4/CD20/CK and DAPI; (F) CD8 (C8/144B, aqua); (G) CD68 (514H12, yellow); (H) PD-L1 (SP263, red); and (I) CK (AE1/AE3, green); and (J) composite CD8/CD68/PD-L1/CK and DAPI. All images are $\times 20$ magnification. FFPE, formalin-fixed, paraffin-embedded.

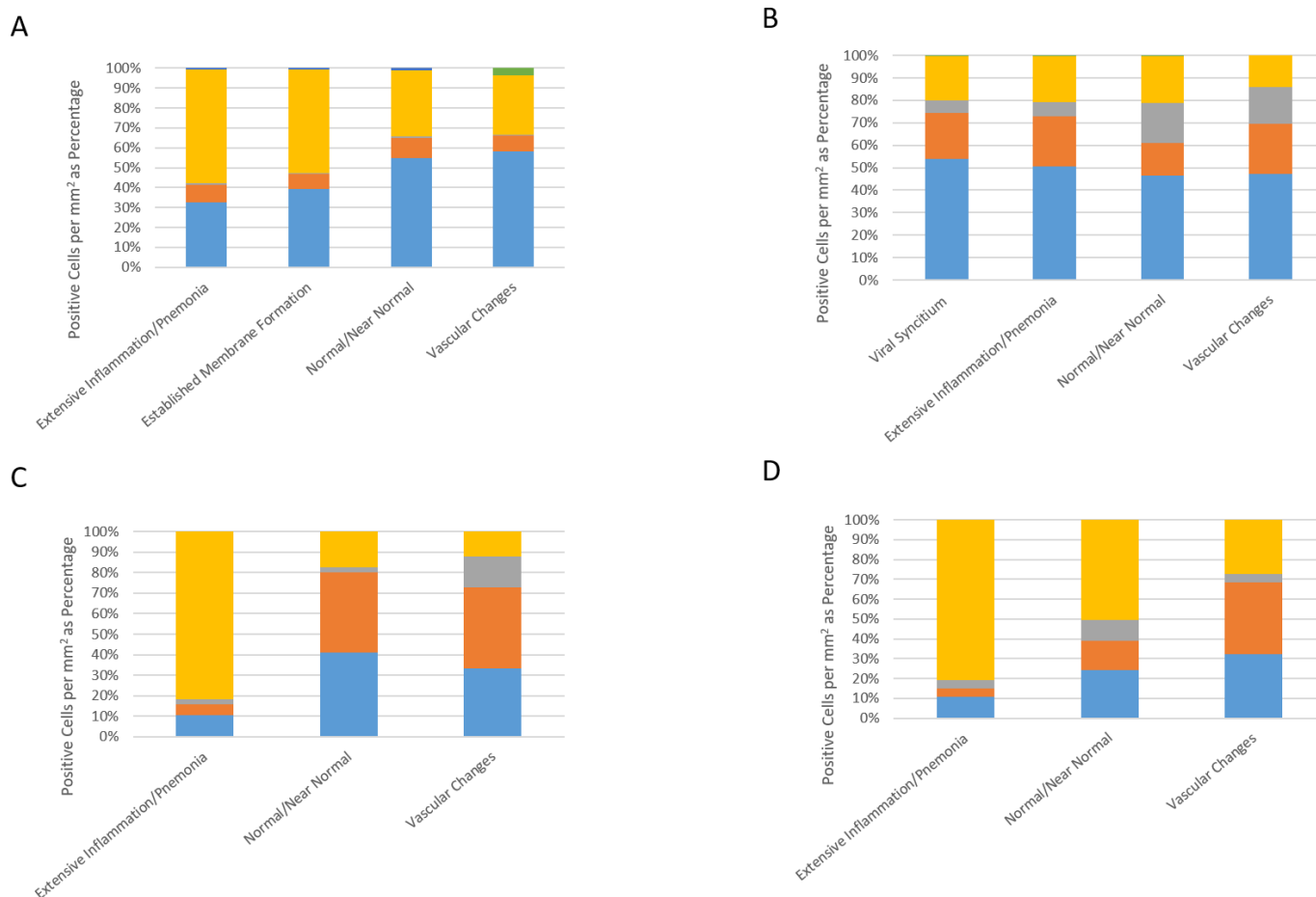


Figure 6 Bar graphs representing the density of immune cells per square millimetre represented as a percentage in COVID-19-positive and COVID-19-negative cases. Areas of normal/near normal, viral syncytium, extensive inflammation/pneumonia, vascular changes and established hyaline membrane formation are shown for (A) case 1, (B) case 2, (C) case 3 and (D) case 4. CD3, blue; CD4, orange; CD8, grey; CD68, yellow; CD20, green.

(figure 6). These changes in immune cell phenotype across ROIs was as much as fivefold different (online supplemental figure S2).

The diversity of phenotypes when comparing SARS-CoV-2 positive cases with non-SARS-CoV-2 cases, in ROIs of vascular change is striking. Across all immune cells assessed (CD3, CD4, CD8, CD68 and D20), SARS-CoV-2-positive cases had a far higher total positive cell density compared with non-SARS-CoV-2 cases (positive cases 1 and 2: 909.6 mm² and 801.23 mm², respectively. Non-SARS-CoV-2 cases 3 and 4: 100.1 and 140.1 mm², respectively).

Taken together, the T-cell and macrophage expressions seen within the vascular change ROIs in SARS-CoV-2 versus non-SARS-CoV-2 are also contrasting. In SARS-CoV-2-positive cases, there was a combined CD3 density of 904.62 mm² (527.6 and 377.01 mm² in each case), yet in both non-SARS-CoV-2 cases, the density of CD3 was greater than 10 times lower at 78.41 mm² (33.36 and 45.05 mm² in each case). This dichotomy in inflammation in SARS-CoV-2 versus non-SARS-CoV-2 cases was observed across immune markers: CD4 (255.48 mm² vs 90.11 mm²), CD8 (113.52 mm² vs 21.21 mm²) and CD68 (383.51 mm² vs 50.45 mm²).

We only observed an identifiable increase in expression of B cells in one SARS-CoV-2-positive case. Case 1, in comparison to areas of normal/near normal (normal: 5.9 mm², vascular change 33.7 mm²) showed a 570% increase in expression. While this was not observed in case 2, this may be explained by

a contrasting clinical time course of COVID-19 between each patient. CD20 expression was not seen in non-COVID-19 cases. For each biomarker in the two multiplex panels, individual cells were identified with the same sensitivity and specificity as we have observed in lung cancer tissue studies.

DISCUSSION

The diagnostic testing of COVID-19 is primarily PCR based on upper respiratory tract samples, or ELISA-type blood based.⁹ Our validation suggests tissue hybridisation detection of SARS-CoV-2 could be reliably used but may be sensitive to disease stage. This may explain the lack of detectable in situ SARS-CoV-2 hybridisation signal in one of the two COVID-proven autopsy samples tested.

The validation of multiplexing analyses, originally developed in our laboratory in the context of oncology,^{7 8 10} enables the opportunity to illuminate the immune microenvironment of COVID-19 related changes. Our results indicate that there is significant variation in the immune reaction in different areas within affected lungs. In addition, our digital pathology approach allows identification of these changes of up to fivefold. While our observations indicate increased immune cells in COVID-19-positive autopsy cases in comparison to samples from non-COVID-19 autopsies, we cannot conclude that viral infection by COVID-19 ultimately leads to an increase in immune response over and above other viral infections. Indeed, studies have

demonstrated that T-cell suppression may be due to increased immune checkpoints (CTLA4, PD-L1 and IDO-1),⁹ as well as those detected in active disease in soluble blood (TIM3 and LAG3). The being said, immune response to COVID-19 infection remains poorly understood, and our data, while limited, is in line with others, which is suggestive of a heightened immune response,¹¹ while several conflicting studies demonstrate T-cell exhaustion.¹² Very few published studies have used mIF to help describe the pathology of COVID-19, primarily to describe the immune response associated with vasculature.¹³

This work demonstrates a proof of principle methodology to capture the immune microenvironment in COVID-19-positive tissues. Further, we establish that the immune microenvironment in COVID-19 autopsy tissue is detectable and quantifiable. Our data indicate that quantification of the immune response to COVID-19 can be achieved within a routine molecular pathology laboratory and, once adapted to clinical samples other than resections (such as materials from biopsies and cytologies), would lend itself to screening of routine diagnostic biopsy samples.

Handling editor Runjan Chetty.

Twitter Matthew Phillip Humphries @DrMattHumphries

Acknowledgements We kindly thank Thijs Kuiken and Rik De Swart, Erasmus University Medical Centre, Rotterdam, Netherlands, for the gift of positive control tissue sections of SARS-CoV-2-infected macaque lung tissue. Some of the samples used in this research were received from the Northern Ireland Biobank, which has received funds from HSC Research and Development Division of the Public Health Agency in Northern Ireland and the Friends of the Cancer Centre.

Contributors Conceptualisation: MPH, SMcQ, DRJS and MS-T. Methodology: MPH, VB, FAIS, SC, BL, HE-d, NO'D, SMcQ, JL, DRJS, JJ and MS-T. Materials: BL, HE-d, ND, CL, JL and JJ. Data analysis: MPH, VB, FAIS, SC and PM. Data curation: MPH, FAIS and PM. Formal analysis: MPH, SMcQ and MS-T. Writing (original draft preparation): MPH. Writing, review and editing: VB, SC, PM, CL, SMcQ, DRJS, JJ and MS-T. Project administration and funding acquisition: JJ and MS-T.

Funding This paper is supported by the PathLAKE Centre of Excellence for digital pathology and artificial intelligence, which is funded from the Data to Early Diagnosis and Precision Medicine strand of the government's Industrial Strategy Challenge Fund, managed and delivered by Innovate UK on behalf of UK Research and Innovation.

Competing interests MS-T is a scientific advisor to Mindpeak and Sonrai Analytics, and has received honoraria recently from BMS, MSD and Incyte. None of these disclosures are related to this work.

Patient consent for publication Not applicable.

Ethics approval This study involves human participants and was approved by the Northern Ireland Biobank (reference NIB20-0329), Arden Tissue Bank UHCW NHS Trust (reference number 18/SC/0180 ATB20-06), Faculty REC (reference number MHLS 20_69). The biopsy samples used in this research were received

from the Northern Ireland Biobank, which has ethical approval to use retrospective deidentified tissue samples from the Belfast Health and Social Care Tissue Pathology archive (REC:11/NI/0013).

Provenance and peer review Not commissioned; externally peer reviewed.

Supplemental material This content has been supplied by the author(s). It has not been vetted by BMJ Publishing Group Limited (BMJ) and may not have been peer-reviewed. Any opinions or recommendations discussed are solely those of the author(s) and are not endorsed by BMJ. BMJ disclaims all liability and responsibility arising from any reliance placed on the content. Where the content includes any translated material, BMJ does not warrant the accuracy and reliability of the translations (including but not limited to local regulations, clinical guidelines, terminology, drug names and drug dosages), and is not responsible for any error and/or omissions arising from translation and adaptation or otherwise.

Open access This is an open access article distributed in accordance with the Creative Commons Attribution 4.0 Unported (CC BY 4.0) license, which permits others to copy, redistribute, remix, transform and build upon this work for any purpose, provided the original work is properly cited, a link to the licence is given, and indication of whether changes were made. See: <https://creativecommons.org/licenses/by/4.0/>.

ORCID iD

Matthew Phillip Humphries <http://orcid.org/0000-0003-1306-7012>

REFERENCES

- 1 World Health Organization. Coronavirus disease 2019 (COVID-19) situation report 67. Available: <https://www.who.int/emergencies/diseases/novel-coronavirus-2019/situation-reports> [Accessed 30 Mar 2020].
- 2 Barth RF, Xu X, Buja LM. A call to action: the need for autopsies to determine the full extent of organ involvement associated with COVID-19. (1931-3543 (electronic)).
- 3 BA-OX R, Kuiken TA-O, Herfst SA-O. Comparative pathogenesis of COVID-19, MERS, and SARS in a nonhuman primate model. (1095-9203 (electronic)).
- 4 Lewis C, McQuaid S, Clark P, et al. The Northern Ireland Biobank: a cancer focused Repository of science. *Open J Bioresour* 2018;5.
- 5 Bankhead P, Loughrey MB, Fernández JA, et al. QuPath: open source software for digital pathology image analysis. *Sci Rep* 2017;7:16878.
- 6 Viratham Pulsawatdi A, Craig SG, Bingham V, et al. A robust multiplex immunofluorescence and digital pathology workflow for the characterisation of the tumour immune microenvironment. *Mol Oncol* 2020;14:2384-402.
- 7 Humphries MP, Bingham V, Abdullahi Sidi F, et al. Improving the diagnostic accuracy of the PD-L1 test with image analysis and multiplex hybridization. *Cancers* 2020;12. doi:10.3390/cancers12051114. [Epub ahead of print: 29 Apr 2020].
- 8 Humphries MP, Craig SG, Kacprzyk R, et al. The adaptive immune and immune checkpoint landscape of neoadjuvant treated esophageal adenocarcinoma using digital pathology quantitation. *BMC Cancer* 2020;20:500.
- 9 Dinnes J, Deeks JJ, Adriano A, et al. Rapid, point-of-care antigen and molecular-based tests for diagnosis of SARS-CoV-2 infection. *Cochrane Database Syst Rev* 2020;8:CD013705.
- 10 Abdullahi Sidi F, Bingham V, Craig SG, et al. PD-L1 multiplex and quantitative image analysis for molecular diagnostics. *Cancers*;13:29.
- 11 Zhang B, Zhou X, Qiu Y. Clinical characteristics of 82 death cases with COVID-19. *medRxiv* 2020:2020.2002.2026.20028191.
- 12 Diao B, Wang C, Tan Y, et al. Reduction and functional exhaustion of T cells in patients with coronavirus disease 2019 (COVID-19). *Front Immunol* 2020;11.
- 13 Dorward DA-O, Russell CA-O, IH U. Tissue-Specific immunopathology in fatal COVID-19. (1535-4970 (electronic)).

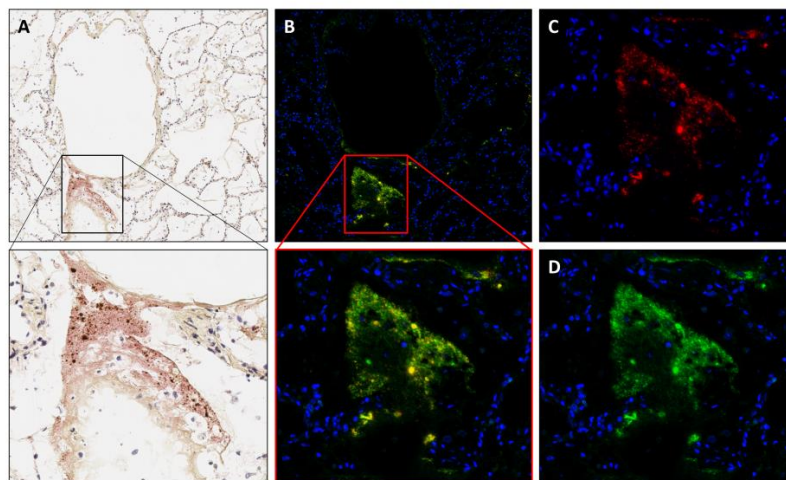
Supplementary Data 1

Case 1 had a short clinical course of 5 days. This late 40s lady had a history of asthma and feeling generally unwell for several days. She was a health care worker who felt the symptoms of COVID-19 (pyrexia and cough) and was self isolating. She was found collapsed on her bedroom floor and, despite resuscitation attempts, was pronounced dead on the same day. The autopsy identified pleural and pericardial effusion, as well as a lung histology dominated by extensive hyaline membrane disease /diffuse alveolar damage (DAD) and pulmonary oedema. Virology tests proved positive for SARS-CoV-2 on both the swabs from the nose and mouth and the lower bronchial tree.

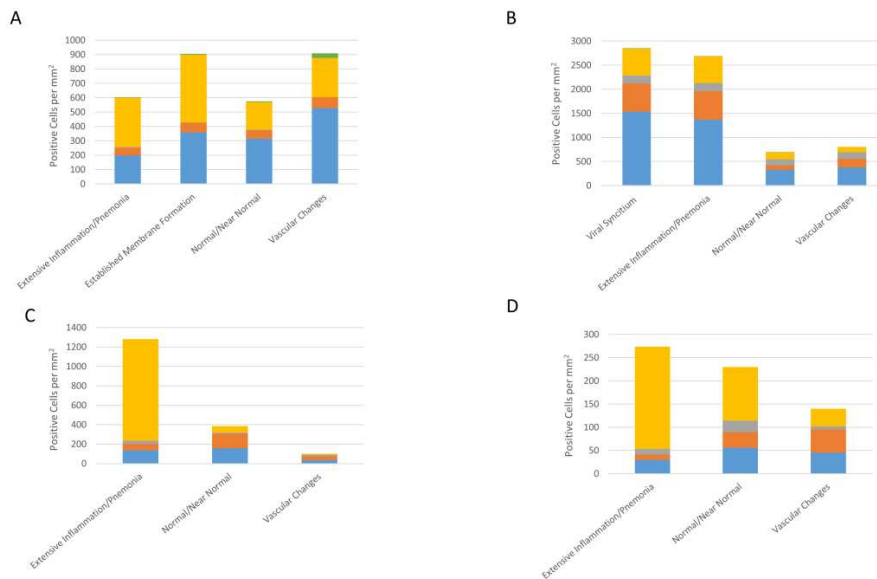
Case 2 is an late 80s gentleman admitted to hospital with cough and breathlessness. Subsequently diagnosed with COVID-19 by PCR. During the admission he developed acute kidney failure and a deep vein thrombosis. Managed on the ward with oxygen and fluid balance and doxycycline. Entered into recovery trial, but his condition deteriorated suddenly and died 13 days post admission. The autopsy found pneumonia, left ventricular hypertrophy, coronary artery atherosclerosis and a swollen left leg in keeping with deep vein thrombosis. The lung histology showed DAD of fibrotic stage, focal bronchopneumonia, isolated foci of thrombosis in small capillary sized vessels and focal re-epithelialization of alveolar spaces with squamous metaplasia. Figure 1 illustrates the complex pathology of this case, with an overall impression of the lung damage (1A); evidence of florid viral syncytial formation (1B); end-stage diffuse alveolar damage with re-epithelization (1C); vascular changes (1D); and a relatively unaffected area of lung parenchyma for comparison (1E).

Case 3 was a diabetic patient with mental health issues, found dead at home and with macroscopic and histological evidence of pneumonia on autopsy.

Case 4 presented to the forensic pathology team with past medical history of pneumonia, anxiety and depression. At autopsy he had an acute pneumonia and emphysema, confirmed by histology, in an overall state of malnourish.



Supplementary Figure S1. (A) IHC and RNAScope Dual-plex DAB x10, with exploded view x20. (B) IHC and RNAScope dual-plex mIF x10, with exploded view x20. (C) mIF single channel displaying RNAScope only (Red) with DAPI counter stain (Blue) x20. (D) mIF single channel displaying IHC only (Green) with DAPI counter stain (Blue) x20.



Supplementary Figure S2. (A) Case 1. (B) Case 2. (C) Case 3. (D) Case 4. CD3 – blue, CD4 – orange, CD8 – grey, CD68 – yellow, CD20 – green.

Multiplex Panel	Biomarker	Clone	Source	Catalogue Number	Epitope Retrieval	Dilution	Incubation	Detection Chemistry
Panel 1	CD3	2GV6	Ventana	5278422001	ER1 30 minutes	1 in 6	30 minutes at ambient	Opal 520
Panel 1	CD4	SP35	Ventana	5552737001	ER1 30 minutes	1 in 4	30 minutes at ambient	Opal 620
Panel 1	CD20	L26	Dako	M0755	ER1 30 minutes	1 in 400	30 minutes at ambient	Opal 570
Panel 2	PD-L1	SP263	Ventana	740-4907	ER2 20 minutes	1:2	30 minutes, ambient	Opal 520
Panel 2	CD8	C8/144B	Dako	M7103	ER2 20 minutes	1 in 400	30 minutes, ambient	Opal 690
Panel 2	CD68	514H12	Novocastra	NCL-L-CD68	ER2 20 minutes	1 in 200	30 minutes at ambient	Opal 570
Panel 2	CK	AE1/AE3	Dako	M3515	ER2 20 minutes	1 in 100	30 minutes at ambient	Opal 620

Table S1 – Antibody details and optimised retrieval methods